

# Excitonic Resonances in Coherent Anti-Stokes Raman Scattering from Single Wall Carbon Nanotubes

Georgy Gordeev,<sup>1,2,3,\*</sup> Lucas Lafeta,<sup>2,4</sup> Benjamin Scott Flavel,<sup>5</sup> Ado Jorio,<sup>2</sup> and Leandro M. Malard<sup>2,†</sup>

<sup>1</sup>*Freie Universität Berlin, Department of Physics, Arnimallee 14, 14195 Berlin*

<sup>2</sup>*Departamento de Física, Universidade Federal de Minas Gerais,  
Belo Horizonte, Minas Gerais 30123-970, Brazil*

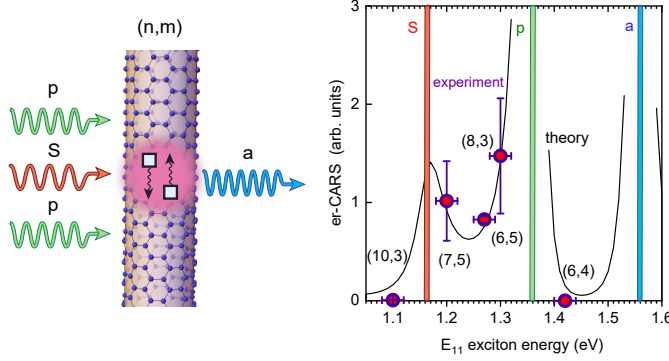
<sup>3</sup>*Department of Physics and Materials Science,  
University of Luxembourg, L-4422 Belvaux, Luxembourg*

<sup>4</sup>*Ludwig-Maximilians-Universität München,  
Department of Chemistry and Center for NanoScience (CeNS),  
Butenandtstraße 5-13 (E), 81377 Munich, Germany*

<sup>5</sup>*Institute of Nanotechnology, Karlsruhe Institute of Technology,  
76201 Eggenstein-Leopoldshafen, Germany*

## Abstract

In this work we investigate the role of exciton resonances in coherent anti-Stokes Raman scattering (er-CARS) in single walled carbon nanotubes (SWCNTs). We drive the nanotube system in simultaneous phonon and excitonic resonances, where we observe a superior enhancement by orders of magnitude exceeding non-resonant cases. We investigated the resonant effects in five  $(n, m)$  chiralities and find that the er-CARS intensity varies drastically between different nanotube species. The experimental results are compared with a perturbation theory model. Finally, we show that such giant resonant non-linear signals enable rapid mapping and local heating of individualized CNTs, suggesting easy tracking of CNTs for future nanotoxicology studies and therapeutic application in biological tissues.



## INTRODUCTION

Raman spectroscopy has been extensively used to characterize materials and biological specimens, however the Raman effect is intrinsically weak due to the small its scattering cross-sections<sup>1–5</sup>. Such low signals prevents the application of the technique for rapid imaging of biological cells, tissues and in-vivo applications<sup>2,5</sup>. On the other hand the use of non-linear optical effects that are in resonance with vibrational states such as Coherent Anti-Stokes Raman Spectroscopy and Stimulated Raman Scattering have been recently used to overcome the weak signals in conventional Raman Spectroscopy. The application of such techniques in combination with nanomaterials may open new avenues in tracking and therapy applications<sup>3,4</sup>. In this sense, single walled carbon nanotubes (SWCNTs) are known to easily penetrate the living cells due to their unique aspect ratio<sup>6</sup>. Here we show that by simultaneously driving the SWCNTs into resonance with exciton and phonon states, the CARS intensity in the SWCNTs is increased by orders of magnitude exceeding non-resonant case. Moreover we studied different nanotube chiralities and find that the CARS enhancement is sensitive to the energy of excitonic resonance, which is modelled by a perturbation theory. In order to explore applicability of CNTs for tracking or future nanotoxicology studies<sup>7</sup> and therapeutic applications<sup>8</sup>, we show that by scanning individual tubes deposited on transparent substrate we can achieve  $16 \mu\text{s}$  per pixel imaging rates; and that the nanotubes can be heated locally by increasing the laser powers up to  $200^\circ\text{C}$  for therapeutic applications.

Coherent anti-Stokes Raman scattering (CARS) can be interpreted as a four-wave mixing (FWM) process which is resonant with a phonon. It combines four photons, two of equal energy (pump) and one lower energy (Stokes) incident in the sample and the fourth photon emerging out of it. In CARS, the energy difference between the Pump and Stokes

beams are tuned to match a specific vibrational mode, therefore enhancing the FWM signal by the anti-Stokes process<sup>1,2</sup>. Furthermore if one of the beams matches real excitonic or electronic transition, the CARS process becomes electronically (excitonically) resonant, we refer to as excitonic resonant CARS (er-CARS)<sup>9</sup>. Such methodology has been successfully applied to molecules improving significantly the detection sensitivity of the induced Raman signal<sup>10</sup>. Due to quantum confinement, nanomaterials can have narrow bandwidth excitonic resonances and thus are promising candidates for resonant er-CARS effects, however such application has been so far been limited. For example CARS has been used to probe nanomaterials inside biological specimens but without the use of resonant effects. In the case of 2D materials, the broad electronic contribution of graphene leads to the interference between the FWM and CARS signals, making it hard to use such technique for imaging proposes<sup>4,11,12</sup>. On the other hand, the optical properties of semiconducting SWCNTs are dictated by the excitonic properties only, with single particle contributions being negligible.

Single walled carbon nanotubes are tubular structures, where one dimensional confinement yields excitonic states with high energy<sup>13</sup> phonons of  $\sim 0.19$  eV with large exciton-phonon coupling.<sup>14,15</sup> For instance, this reflects in high resonance Raman cross sections,<sup>16,17</sup> where single tubes can be experimentally measured by Raman spectroscopy<sup>18,19</sup>. The linear absorption of CNTs is dominated by sharp excitonic resonances at room temperature which are determined by the nanotube chiral indices.<sup>20</sup> CARS has been used to study carbon nanotubes, either using raw soot ensembles of chiralities<sup>21,22</sup> or individual tube grew by chemical vapor deposition<sup>23,24</sup>. In both cases the excitonic resonant states were not well defined since the CNT were not single chirality and therefore the electronic states were overlapped. Recently the chirality separation techniques became available that can enrich a pure single chirality<sup>25-27</sup>. Here we show that such samples allow the use of er-CARS in resonance with excitons in SWNT.

## EXPERIMENTAL METHODS

The nanotube *chirality enriched samples* (8,3), (6,4), (7,5) SWCNTs were prepared using gel permeation method<sup>26</sup> and the (10,3) SWCNTs using gel chromatography<sup>25</sup>. The (6,5) SWCNTs were prepared from HiPco raw material (NanoIntegris) as outlined previously using a gel permeation chromatography system.<sup>26,27</sup> Due to the high affinity of (6,5) to the

Sephacryl-S200 gel (Amersham Biosciences) and their ability to displace other (n,m) species at 1.6 wt % SDS (Merck), 1 wt % sodium cholate (SC,  $\gtrsim 99$  %, Sigma Aldrich) was used as an eluent in a one column approach without the use of a pH gradient. The nanotube suspension was drop cased onto the thin quartz substrate. The dried samples was put in a water beaker overnight to remove surfactant residues. For *resonant CARS measurements*, a picosecond laser (APE PicoEMERALD) was used. This laser system generated two laser beams that can be spatially and temporally overlapped with wavelengths at 1064 nm ( $E_S$ ) with 7 ps pulse duration and the second tunable between 730 and 960 nm ( $E_p$ ) with 5–6 ps pulse duration. The  $E_p$  and is generated by pumping the optical parametric oscillator cavity with the second harmonic of the 1064 nm laser at 532 nm. The selected  $E_p$ ,  $E_S$ , lasers were directed to the sample by mirrors. The collection and detection parts were separated by a beam-splitter, afterwards the anti-Stokes signal  $E_a$  was filtered by a short-pass filter and focused on a spectrometer slit of the spectrometer (Andor Shamrock SR-303i-B) equipped with a charge-coupled device (iDus DU420A-BEX2-DD). The laser powers on the sample were kept below  $\sim 0.5$  mW for resonant experiments shown in Figures 2, 3. Only in the measurement shown in Figure 5 higher laser power was used.

Same detection setup was used for *Raman measurements*, but for sample excitation the diode laser at 561 nm was used combined with a long-pass filter in order to separate Raman from Rayleigh scattering. For simultaneous measurements with Raman and CARS the visible and IR beams were aligned together using a beam splitter and focused onto the same spot on a sample.

In order to *calibrate er-CARS intensity* we need to account for difference in laser power used and for different CNTs concentration under the laser spot. The CARS signals are proportional to  $P_{tot} = I_p^2 I_S$ , therefore the integrated intensity of the CARS was first divided by  $P_{tot}$ . In order to determine the concentration of the CNTs under the laser spot we utilize Raman spectroscopy. When the laser energy matches the transition energy, the G mode Raman intensity of one individual CNT is predicted to weakly depend on chirality and diameter, due to similarity in matrix elements.<sup>15</sup> We account for different resonance energies between (n,m) by introducing an intensity factor  $f_{Ram}$ .  $f_{Ram}$  depends on energy difference between  $E_{22}$  and  $E_{las}$ . For the G mode this dependence is chirality specific, but is known from previous experiments for all the species accept for the (10,3) SWCNTs, where we approximate it to the (8,3) SWCNTs.<sup>28,29</sup> The CNTs concentration  $C$  is then  $I_{Ram} f_{Ram}$ .

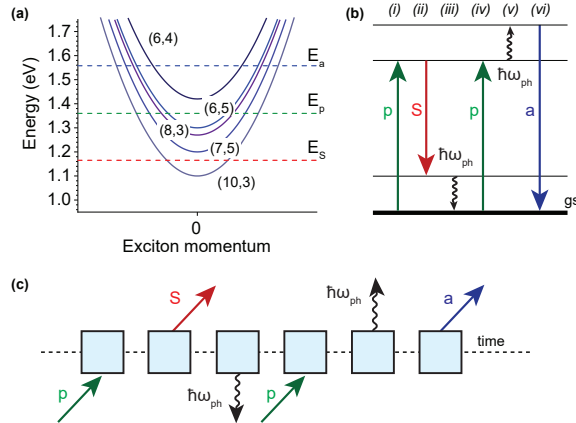


FIG. 1. The concept of the er-CARS scattering in SWCNTs. (a) Exciton dispersion for different (n,m) SWNT probed in this study, along with fixed energies of pump ( $E_p$ ), Stokes ( $E_S$ ), and anti-Stokes beams ( $E_a$ ). (b) Scheme of one er-CARS scattering pathway in an excitonic system. (c) Feynman diagram representing sixth-order process, straight (curly) arrows indicate an interaction with a photon (phonon), see discussion in text for possible permutations.

Finally, the Raman intensity scales with  $\sim C$ , but CARS intensity is proportional to the  $C^2$ . In order to show resonant effects we then calibrate  $I_{CARS}$  as  $I_{CARS}^{measured}/P_{tot}/C^2$ , accounting for laser powers and different concentrations. The error bars in Figure 4 were computed using standard error propagation methods and is mainly due to uncertainty in the estimation of the  $E_{22}$  transition energy influencing the resonant factor of Raman scattering.

For the CARS intensity image, we have redirected the ( $E_S$ ) and  $E_p$  pulses to a scanning laser microscope (LaVision Biotec). The scanning mirrors allow the beams to map the sample when focused by the  $60\times$  apochromatic air objective (numerical aperture of 0.95) in the scanning laser microscope. The backscattered CARS signal is then directed to the photomultiplier. A short pass filter eliminates laser contamination. The average scan contained  $10^6$  pixels and was completed within 16s.

## RESULTS

Four-wave mixing comprises interaction of four photons energies, the incident three photons can excite or deexcite the system yielding an emission of the fourth one. We use the first and third photons of the same energy  $E_p$ , Pump beam. The second photon has a smaller

energy  $E_S$ , Stokes beam. The energy of the fourth, anti-Stokes photon is pre-determined by the first three and yields  $E_a = 2E_p - E_S$ <sup>1</sup>. The energy of the Stokes beam is kept constant  $E_S = 1.165$  eV whereas the energy of the pump beam is tunable. A single vibration of the system can be resonantly excited by matching the energy  $E_p - E_S$  with phonon energy  $E_{ph}$ <sup>2</sup>. Intuitively one would expect a more efficient CARS process whenever the  $E_i$ , ( $i = p, S, a$ ) meets excitonic resonance of the nanotube (er-CARS). The photon energies for  $E_p$ ,  $E_S$  and  $E_a$  are compared with the exciton energies used in Figure 1a, where it is possible to observe different resonances. We therefore need a model to describe the influence of resonant states explicitly<sup>1</sup>.

Historically, four-wave mixing was mostly studied in zero dimensional systems, such as molecules. In such systems the excitonic and vibrational states are equal in treatment, and a density matrix approach is typically used to describe non-linear interactions with light.<sup>30</sup> However, in solid state systems the excitonic and phonon states are independent quasi-particles and this approach is not as applicable<sup>31</sup>. Instead, the interaction between phonons states and electronic excitation occurs via electron-phonon Hamiltonian, where the electron (exciton) can be scattered to a new state either by creating or emitting a phonon. In a similar fashion, excitons can be scattered to new states by photon absorption or emission through the exciton-photon interaction. To understand the interplay between different matrix elements we turn to the perturbation theory, widely used to describe resonant Raman processes.<sup>31</sup>

Figure 1b depicts one possible CARS scattering process, where the energy difference between Pump and Stokes equals an optical phonon energy. The same process is shown in Figure 1c in form of a Feynman diagram. Each vertex of the Feynman diagram represents an interaction with either photon or phonon and the vertices are ordered in time. An arrow pointing to the system represent energy increase, whereas an arrow pointing away from the system represents an energy decrease. The phonon creation and eliminations occur at the vertices two and five, respectively. By walking through the steps first (*i*) we see that the system is excited by the  $E_p$ . Later on (*ii*) the interaction with a negative component of  $E_S$  electric field deexcites the system towards the ground state and (*iii*) the phonon is created  $E_{ph}$ . Next the third photon  $E_p$  excites the system into higher state (*iv*) and after it, the phonon that was created before is destroyed (*v*). Finally, fourth wave photon emerges out of the system (*vi*), bringing system back to the ground state, which satisfies energy conservation principle, build in into the perturbation theory.

Quantum interference between many scattering processes determines the total er-CARS signal enhancement. Overall, there are 43 pathways that can be obtained by changing order of the scattering events. To select them from full permutation group consisting of  $6!/2!$  members we use one physical constrain. At any step of the process the total system energy is not allowed to drop below the energy of the ground state. We impose the phonon emission and scattering to be equally probable, since a large amount of photons are incident on the sample during a pico-second laser pulse. Each of the 43 process contributes to the er-CARS intensity at the same time with equal probability yielding an interference effect:

$$I_{rCARS} = \left[ \sum_k^{43} I_k \right]^2, \quad (1)$$

where  $I_k$  is the contribution of a  $k$ -th scattering pathway. The square is taken after summation allowing the processes to interfere. The  $I_k$  can be expressed as:

$$I_k(E_{11}[n, m]) = \frac{M_{ex-q}^2 (M_{ex-ph})^4}{\prod_{l=1}^5 (E_{11}[n, m] + \sum_i^l \pm \hbar\omega_i - I\gamma_{11})}. \quad (2)$$

The  $M_{ex-ph}$  is exciton-photon and  $M_{ex-q}$  is exciton-phonon matrix elements,  $\hbar\omega_i$  is the energy interacting at the  $i$ -th vertex, either photon( $E_p, E_S, E_a$ ) or phonon  $E_{ph}$ .  $\gamma_{11}$  is the broadening factors related to the excitonic lifetime. The sign of the  $\hbar\omega_i$  is determined by the direction of the arrow, either pointing away or towards the system in a Feynman diagram, see example in Figure 1c. For one possible process these energies are depicted in Figure 1b, c. From Eq. (1) we expect that resonant enhancement of the CARS process, when either one of three involved photons is close to the energy of the exciton. We can verify this experimentally by using different nanotube chiralities (n,m), which would enter Eq. (2) as  $E_{11}[n, m]$ . While (n,m) chiralities with  $E_{11}$  exactly matching  $E_p$  will provide high enhancement, the most interesting interference effects happen in between  $E_S$  and  $E_a$ . We therefore focus on (n,m) chiralities in this range.

Vibrational enhancement is superior for the longitudinal phonon, compared to the transverse one. We investigate the effect of vibrational enhancement in (6,5) nanotube. Figure 2a shows the FWM signal for the (6,5) SWNT for several pump energies ( $E_p$ ) spanning across vibrational resonance and for a fixed Stokes energy ( $E_S = 1.164$  eV). When the pump energy approaches 1.362 eV ( $E_p - E_S = 0.197$  eV), which matches well the LO phonon energy of

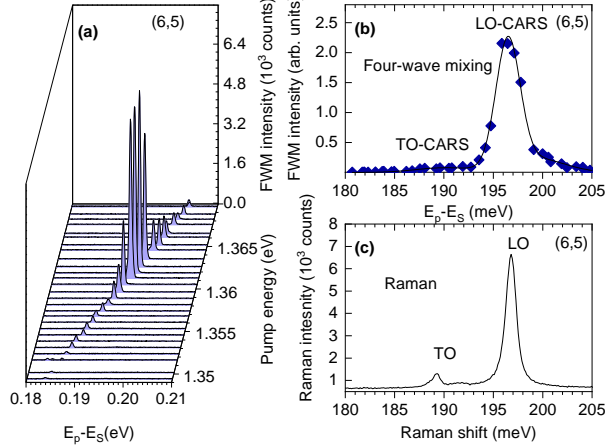


FIG. 2. Four-wave mixing (FWM) in the (6,5) CNT across high energy phonon resonances (G modes). (a) Waterfall plot of the experimental FWM spectra, the  $x$  axis shows difference between anti-Stokes and Pump energies,  $y$  axis represents the pump energy  $E_p$ . (b) Integrated area of the  $E_a$  signal vs phonon energy. (c) Raman scattering intensity comparison between the LO and TO resonances.

the SWNT, the FWM intensity has a gigantic 2000 times enhancement. Such resonance with the LO phonon is shown in Fig. 2b where the the integrated area of the FWM signal is plotted with respect to  $E_p - E_S$  (or  $E_a - E_p$ ). The enhancement reported here much larger than a previously reported 2x on-off resonance contrast to *Kim et al.*<sup>24</sup>. We attribute this to the excitonic resonance effect, discussed in the following paragraphs. We observe a smaller enhancement for the TO phonon with  $E_{TO}$  close to 0.189 eV (see Fig. 2b). The resonant CARS with the LO phonon is  $\sim$ 25 times higher than with TO phonon. On the other hand, in Raman scattering experiments the LO phonon is only 5 times more intense than the TO phonon, see Fig. 2c. Such difference in the LO/TO intensity ratio is well captured by our perturbation theory. Stokes Raman scattering is proportional to  $(M_{ex-q})$ , since the phonon is emitted only once. On the other hand CARS scales as  $(M_{ex-q})^2$ , because the exciton-phonon interaction occurs twice when phonon is created and eliminated, therefore the observed difference for the LO/TO enhancement factor fits well with this theoretical interpretation.

The phonon linewidth is slightly different between Raman and four wave mixing. We measure the FWM signal close to the G mode resonances in different nanotube chiralities, with the  $E_{11}$  energy spanning between 1.1 eV in (10,3) SWCNTs and 1.42 eV in (6, 4) CNTs,

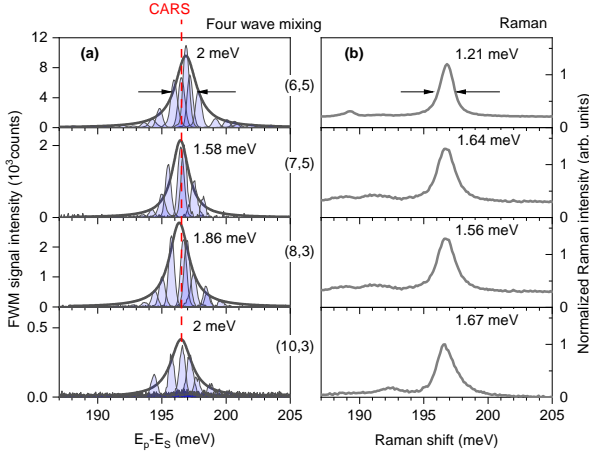


FIG. 3. Four-wave mixing in different  $(n,m)$  CNTs in resonance with the LO phonon. (a) FWM profiles in different chiralities, solid lines are Lorentz fits and their full width at half maxima is given by the numbers near the plot. The Stokes and Pump intensities were 60, 150, 100, 590  $\mu W$ , from top to bottom,  $E_S = 1.165$  eV,  $E_p = 1.35 - 1.37$  eV. (b) Raman spectra taken at the same spot, with laser energy of 2.2 eV.

as shown in Figure 2a. In all the SWCNT chiralities measured, the highest FWM signal was found for resonance with the LO phonon, see red vertical line Figure 3a. The line-shape of the FWM profiles is mainly determined by the lifetime of the phonon as  $\sim \hbar/\tau_{ph}$ . A similar lifetime can be observed in the Raman spectra for the same SWNT as shown in Figure 3b, where the widths of the Raman G band are compared. Overall, the FWM profiles have higher full widths at half maximum (fwhm) than measured by Raman spectroscopy, except for the (7,5) SWCNTs, where the full width are almost identical with a values of 1.6 meV. The difference in linewidths can be explained by higher electronic temperature generated in the case of pulsed laser excitation as shown by previous works on graphene<sup>32</sup>. In such case the CARS linewidth are broader compared to Raman spectroscopy,<sup>11,12,32</sup> where the excitation laser does not create a hot electron temperatures.

The CARS intensity strongly varies between different chiralities due to different resonance conditions. Figure 4 shows the dependence of the enhancement at the LO phonon energy as function of nanotube exciton energy  $E_{11}$ . The CARS intensity is normalized on laser powers  $P_p^2 P_S$  and calibrated by the nanotubes concentration, see Methods. The highest signals was provided by the (7,5), (6,5) and (8,3) SWCNTs, with  $E_{11}$  located between  $E_S$  and  $E_p$ . We did not find any non-linear signal from (6,4) SWCNTs, despite Raman showing

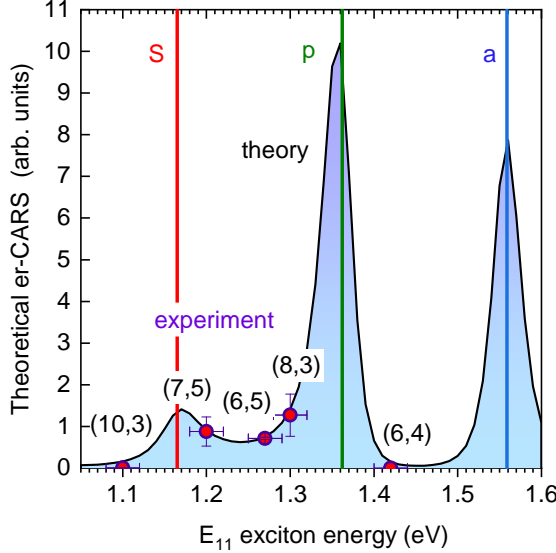


FIG. 4. er-CARS intensities for different  $(n, m)$ . The energies of  $E_p$ ,  $E_S$ , and  $E_a$  are fixed whereas the  $E_{11}$  energy is varied. Symbols represent experimental data, integrated area of the FWM peak normalized on power and nanotube concentration obtained through Raman spectroscopy. The line represents theoretical calculation by Eq. (1) with  $\gamma_{11} = 40$  meV,  $E_S = 1.165$  eV,  $E_p = 1.36$  eV, and  $E_{ph} = 0.196$  eV.

clear signatures of the SWCNT in the measured spot. The  $E_{11}$  of  $(6,4)$  is on the high energy shoulder and lies between  $E_p$  and  $E_a$ . From Figure 4 we can see that experimental er-CARS intensity is not symmetrically distributed between between Stokes, anti-Stokes and Pump energies.

Sixth-order perturbation theory yield asymmetric lineshape, similar to experimental results. The calculated  $I_{FWM}$  is plotted by lines as a function of  $E_{11}$  in Figure 4. The calculation is performed using Eqs. (1) and (2) with constant matrix element approximation and damping factors set to  $\gamma_{11} = 40$  meV, typical for the  $E_{11}$  excitonic transition<sup>33</sup>. The values for the lasers energies are  $E_S = 1.165$  eV,  $E_p = 1.36$  eV, and for the phonon is  $E_{ph} = 0.196$  eV are shown by vertical lines. Figure 4 shows that the er-CARS intensity is enhanced when the  $E_{11}$  transition energies matches either the Stokes, pump or anti-Stokes beam energies. However the distribution of intensities between these peaks is asymmetric due to the interference effect. At lower energies between  $E_S$  and  $E_p$  the interference is positive, whereas at higher energies between  $E_p$  and  $E_a$  the interference is negative and almost

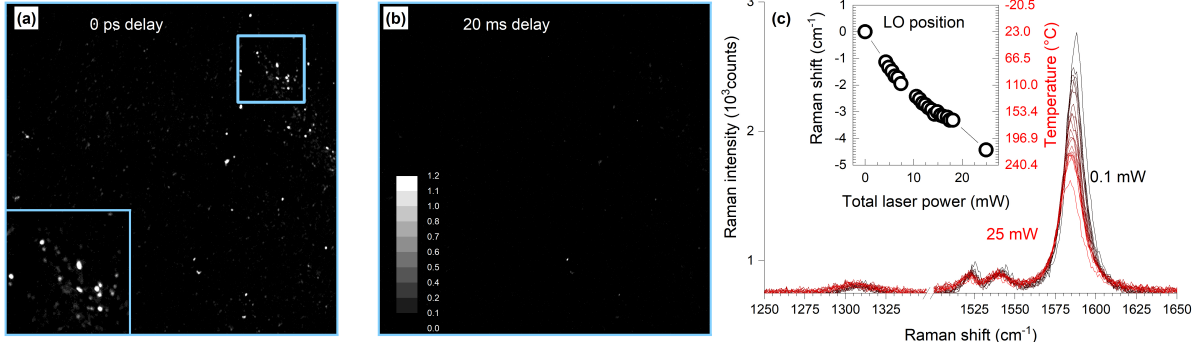


FIG. 5. er-CARS microscopy and local heating of the (6,5) SWCNTs. (a) Lateral spatial maps of the er-CARS signal with zero delay, collected within 16 s ( $E_S = 1.165$  eV,  $E_p = 1.36$  eV). (b) Same image as (a), but scanned with 20 ps delay. (c) Monitoring local temperature by higher irradiation powers in the (6,5) SWCNTs, the Raman excited with 2.2 eV laser. Inset shows Position of the LO phonon as a function of total laser power  $E_p + E_S$ , right scale extracted local temperature using  $-0.023$   $\text{cm}^{-1}/\text{K}$  coefficient.<sup>34</sup>

no er-CARS enhancement is expected. This reproduces well the experimental observations.

We use (6,5) nanotube to perform er-CARS microscopy, since most enriching techniques target that species and shows positive er-CARS interference effects. Figure 5a shows an er-CARS image at the phonon resonance with  $200 \times 200 \mu\text{m}$  in size of (6,5) SWCNTs dropcasted onto a quartz substrate. The bright spots correspond to the individual (6,5) SWCNTs or small bundles. The scan is performed within 16 s. In total  $10^6$  pixels were collected, resulting in average speed of  $16 \mu\text{s}$  per pixel, where that speed is mostly limited by the galvanometric mirrors. We confirm that the bright spots originate from er-CARS process we scanned the same image with a 20 ps delay between the  $E_S$  and  $E_p$  pulses,  $\sim 10$  times  $\tau_{ph}$ . As shown in Figure 5b, the bright spots disappear validating the er-CARS nature of the observed signal. We further tested the 3D imaging option by tuning the focus outside of the quartz surface, see Supplementary Video 1. Out of focus the bright spots clearly loose the intensity and convert to circular shapes, enabling z resolution. Our results show that er-CARS process enables quick and precise localization of SWCNTs in 2D and 3D, enabling its use for imaging CNT in vivo studies, where Raman or photoluminescence signals from individual species are still fairly weak.

The CNTs can be used for the simultaneous er-CARS imaging and local heating the

CNT for targeted destruction of viruses and cancer cells.<sup>35</sup> Most biological tissues have transparency window in the IR region where the  $E_{11}$  transition energies of small-diameter CNTs are found, therefore the heat wave can be localized near the CNT position. Now the temperature control methods rely mostly on mathematical models.<sup>35,36</sup> In our setup we can directly probe and control local temperature, using Raman signal of CNT as a thermometer. We measured the Raman spectrum of a small CNT bundle with during simultaneous irradiation with pulsed  $E_p$  and  $E_S$  beams of varying powers. The Raman spectra are shown in Figure 5c from weak (black) to strong (red) irradiation powers (the measured laser power is the sum of both pump and Stokes beams). Notably, no defects were introduced to the sample, as the D mode doesn't grow in intensity<sup>37</sup>. Further, we observe that the LO phonon broadens and shifts to smaller energies. We plot the LO phonon position as a function of total power  $P_S + P_p$  in the inset of Figure 5c. The Raman shift is converted to temperature by a  $-0.023 \text{ cm}^{-1}/\text{K}$  coefficient<sup>34</sup>. We can easily achieve temperatures close to 200 °C, when even 80 °C will denature the proteins in the living cells<sup>38</sup>. This means that CNT-based er-CARS microscopy is suitable for tracking, local heating, and disruption of the cancer cells.

## CONCLUSIONS

We demonstrated that phonon and excitonic resonances can enhance four-wave mixing signals by few orders of magnitude in SWCNTs giving rise to er-CARS process. We investigated the resonant signals in five different CNT chiralities. The intensity varied drastically and depends upon then relative energy between pump and Stokes beams with respect to the first excitonic transition. We developed a theory based on quantum interference between 43 scattering pathways, which delivered a qualitative agreement with experimental results. Further we tested applicability of resonant wave mixing and imaged individual (6,5) CNTs over  $200 \times 200 \mu\text{m}^2$  quartz substrate in a time of 16 s. The time was only limited by the speed of our galvanometric mirrors and even quicker scans can be achieved in the future. As a possible application the simultaneous er-CARS imaging with local heating with lasers used in CARS could be used for targeting and cell disruption in the future. Our work demonstrates that the single walled carbon nanotubes are highly interesting materials in terms of the resonant non-linear light-matter interaction with potential applications in tracking and

nanotoxicology.

## ACKNOWLEDGMENTS

G.G. gratefully acknowledges the German Research Foundation (DFG via SFB 658, sub-project A6). Dahlem research school (FU bright fellowship) and Focus Area NanoScale of Freie Universitaet Berlin. L.L. gratefully acknowledges the Alexander von Humboldt Foundation for the financial support. B.F. acknowledges DFG grants FL 834/5-1, FL 834/7-1, FL 834/9-1 and FL 834/12-1. L.L, A.J. and L.M.M acknowledges financial support from CNPq, CAPES, FAPEMIG, FINEP, Brazilian Institute of Science and Technology (INCT) in Carbon Nanomaterials and Rede Mineira de Materiais 2D (FAPEMIG). L.M.M. also acknowledges the CAPES and Humboldt fellowship. All authors are thankful for fruitful discussions with Prof. Riichiro Saito and Prof. Stephanie Reich.

---

\* georgy.gordeev@uni.lu

† lmalard@fisica.ufmg.br

- [1] R. Boyd, *Nonlinear Optics* (Academic Press, London, 2008).
- [2] J.-X. Cheng and X. S. Xie, *Coherent Raman Scattering Microscopy* (CRC Press, Boca Raton, FL, 2013).
- [3] R. C. Prince, R. R. Frontiera, and E. O. Potma, Stimulated raman scattering: From bulk to nano, *Chemical Reviews*, Chemical Reviews **117**, 5070 (2017).
- [4] L. M. Malard, L. Lafeta, R. S. Cunha, R. Nadas, A. Gadelha, L. G. Cançado, and A. Jorio, Studying 2d materials with advanced raman spectroscopy: Cars, srs and ters, *Phys. Chem. Chem. Phys.* **23**, 23428 (2021).
- [5] Y. Li, B. Shen, S. Li, Y. Zhao, J. Qu, and L. Liu, Review of stimulated raman scattering microscopy techniques and applications in the biosciences, *Advanced Biology* **5**, 2000184 (2021), <https://onlinelibrary.wiley.com/doi/pdf/10.1002/adbi.202000184>.
- [6] A. E. Porter, M. Gass, K. Muller, J. N. Skepper, P. A. Midgley, and M. Welland, Direct imaging of single-walled carbon nanotubes in cells, *Nature Nanotechnology* **2**, 713 (2007).

[7] R. M. Goodhead, J. Moger, T. S. Galloway, and C. R. Tyler, Tracing engineered nanomaterials in biological tissues using coherent anti-stokes raman scattering (cars) microscopy – a critical review, *Nanotoxicology* **9**, 928 (2015), pMID: 25962086, <https://doi.org/10.3109/17435390.2014.991773>.

[8] K. Kostarelos, A. Bianco, and M. Prato, Promises, facts and challenges for carbon nanotubes in imaging and therapeutics, *Nature Nanotechnology* **4**, 627 (2009).

[9] B. Hudson, W. Hetherington, S. Cramer, I. Chabay, and G. K. Klauminzer, Resonance enhanced coherent anti-stokes raman scattering, *Proceedings of the National Academy of Sciences* **73**, 3798 (1976).

[10] L. Wei and W. Min, Electronic preresonance stimulated raman scattering microscopy, *The Journal of Physical Chemistry Letters*, *The Journal of Physical Chemistry Letters* **9**, 4294 (2018).

[11] L. Lafetá, A. R. Cadore, T. G. Mendes-De-Sa, K. Watanabe, T. Taniguchi, L. C. Campos, A. Jorio, and L. M. Malard, Anomalous Nonlinear Optical Response of Graphene Near Phonon Resonances, *Nano Letters* **17**, 3447 (2017), arXiv:1701.09023.

[12] A. Virga, C. Ferrante, G. Batignani, D. De Fazio, A. Nunn, A. Ferrari, G. Cerullo, and T. Scopigno, Coherent anti-stokes raman spectroscopy of single and multi-layer graphene, *Nature communications* **10**, 1 (2019).

[13] L. Luer, C. Gadermaier, J. Crochet, T. Hertel, D. Brida, and G. Lanzani, Coherent phonon dynamics in semiconducting carbon nanotubes: A quantitative study of electron-phonon coupling, *Physical Review Letters* **102**, 2 (2009).

[14] S. K. Doorn, P. T. Araujo, K. Hata, and A. Jorio, Excitons and exciton-phonon coupling in metallic single-walled carbon nanotubes: Resonance Raman spectroscopy, *Physical Review B - Condensed Matter and Materials Physics* **78**, 1 (2008).

[15] J. Jiang, R. Saito, K. Sato, J. S. Park, G. G. Samsonidze, A. Jorio, G. Dresselhaus, and M. S. Dresselhaus, Exciton-photon, exciton-phonon matrix elements, and resonant Raman intensity of single-wall carbon nanotubes, *Physical Review B - Condensed Matter and Materials Physics* **75**, 10.1103/PhysRevB.75.035405 (2007).

[16] S. Maruyama, R. Xiang, P. G. Etchegoin, E. C. Le Ru, J. E. Bohn, and S. Chiashi, Estimating the Raman Cross Sections of Single Carbon Nanotubes, *ACS Nano* **4**, 3466 (2010).

- [17] C. D. Tschannen, G. Gordeev, S. Reich, L. Shi, T. Pichler, M. Frimmer, L. Novotny, and S. Heeg, Raman Scattering Cross Section of Confined Carbyne, *Nano letters* **20**, 6750 (2020), arXiv:2006.14096.
- [18] A. Jorio, A. G. Souza Filho, G. Dresselhaus, M. S. Dresselhaus, A. K. Swan, M. S. Ünlü, B. B. Goldberg, M. A. Pimenta, J. H. Hafner, C. M. Lieber, and R. Saito, G-band resonant Raman study of 62 isolated single-wall carbon nanotubes, *Physical Review B - Condensed Matter and Materials Physics* **65**, 1554121 (2002).
- [19] S. B. Cronin, A. K. Swan, M. S. Ünlü, B. B. Goldberg, M. S. Dresselhaus, and M. Tinkham, Resonant Raman spectroscopy of individual metallic and semiconducting single-wall carbon nanotubes under uniaxial strain, *Physical Review B - Condensed Matter and Materials Physics* **72**, 35425 (2005).
- [20] R. B. Weisman and S. M. Bachilo, Dependence of optical transition energies on structure for single-walled carbon nanotubes in aqueous suspension: An empirical Kataura plot, *Nano Letters* **3**, 1235 (2003).
- [21] A. Paddubskaya, A. Dementjev, A. Devižis, R. Karpicz, S. Maksimenko, and G. Valušis, Coherent anti-stokes raman scattering as an effective tool for visualization of single-wall carbon nanotubes, *Opt. Express* **26**, 10527 (2018).
- [22] A. S. Duarte, J. Rehbinder, R. R. B. Correia, T. Buckup, and M. Motzkus, Mapping impurity of single-walled carbon nanotubes in bulk samples with multiplex coherent anti-stokes Raman microscopy, *Nano Letters* **13**, 697 (2013).
- [23] T. Sheps, J. Brocious, B. L. Corso, O. T. Gü, D. Whitmore, G. Durkaya, E. O. Potma, and P. G. Collins, Four-wave mixing microscopy with electronic contrast of individual carbon nanotubes, *Physical Review B - Condensed Matter and Materials Physics* **86**, 1 (2012).
- [24] H. Kim, H. Kim, T. Sheps, T. Sheps, P. G. Collins, P. G. Collins, E. O. Potma, and E. O. Potma, Nonlinear optical imaging of individual carbon nanotubes with four-wave-mixing microscopy., *Nano letters* **9**, 2991 (2009).
- [25] H. Liu, D. Nishide, T. Tanaka, and H. Kataura, Large-scale single-chirality separation of single-wall carbon nanotubes by simple gel chromatography, *Nature Communications* 10.1038/ncomms1313 (2011).
- [26] B. S. Flavel, K. E. Moore, M. Pfohl, M. M. Kappes, and F. Hennrich, Separation of single-walled carbon nanotubes with a gel permeation chromatography system, *ACS Nano* **8**, 1817

(2014).

- [27] B. S. Flavel, M. M. Kappes, R. Krupke, and F. Hennrich, Separation of single-walled carbon nanotubes by 1-dodecanol-mediated size-exclusion chromatography, *ACS Nano* **7**, 3557 (2013).
- [28] J. G. Duque, H. Chen, A. K. Swan, A. P. Shreve, S. Kilina, S. Tretiak, X. Tu, M. Zheng, and S. K. Doorn, Violation of the condon approximation in semiconducting carbon nanotubes, *ACS Nano* **5**, 5233 (2011).
- [29] G. Gordeev, A. Jorio, P. Kusch, B. G. Vieira, B. Flavel, R. Krupke, E. B. Barros, and S. Reich, Resonant anti-Stokes Raman scattering in single-walled carbon nanotubes, *Physical Review B* **96**, 245415 (2017).
- [30] S. Mukamel, *Principles of Nonlinear Optical Spectroscopy*, Oxford series in optical and imaging sciences (Oxford University Press, 1999).
- [31] P. Y. Yu and M. Cardona, *Fundamentals of Semiconductors – Physics and Materials Properties* (Springer, Berlin Heidelberg, 1995) arXiv:arXiv:1011.1669v3.
- [32] C. Ferrante, A. Virga, L. Benfatto, M. Martinati, D. De Fazio, U. Sassi, C. Fasolato, A. K. Ott, P. Postorino, D. Yoon, G. Cerullo, F. Mauri, A. C. Ferrari, and T. Scopigno, Raman spectroscopy of graphene under ultrafast laser excitation, *Nature Communications* **9**, 10.1038/s41467-017-02508-x (2018), arXiv:1704.00186.
- [33] G. Gordeev, B. Flavel, R. Krupke, P. Kusch, and S. Reich, Asymmetry of resonance Raman profiles in semiconducting single-walled carbon nanotubes at the first excitonic transition, *Physical Review B* **99**, 45404 (2019).
- [34] Y. Ouyang and Y. Fang, Temperature dependence of the raman spectra of carbon nanotubes with 1064 nm excitation, *Physica E: Low-Dimensional Systems and Nanostructures* **24**, 222 (2004).
- [35] L. Golubewa, I. Timoshchenko, O. Romanov, R. Karpicz, T. Kulahava, D. Rutkauskas, M. Shuba, A. Dementjev, Y. Svirko, and P. Kuzhir, Single-walled carbon nanotubes as a photo-thermo-acoustic cancer theranostic agent: theory and proof of the concept experiment, *Scientific Reports* **10**, 10.1038/s41598-020-79238-6 (2020).
- [36] G. Eskiizmir, A. T. Ermertcan, and K. Yapici, Nanomaterials: Promising structures for the management of oral cancer, *Nanostructures for Oral Medicine* , 511 (2017).
- [37] G. Gordeev, A. Setaro, M. Glaeske, S. Jürgensen, and S. Reich, Doping in covalently functionalized carbon nanotubes: A Raman scattering study, *Physica Status Solidi (B)* **253**, 2461

(2016).

[38] Y. W. Chen, Y. L. Su, S. H. Hu, and S. Y. Chen, Functionalized graphene nanocomposites for enhancing photothermal therapy in tumor treatment, *Advanced Drug Delivery Reviews* **105**, 190 (2016).